JGR Earth Surface

RESEARCH ARTICLE
10.1029/2022JF006875

Estimating the Age of Abandoned Alluvial Surfaces Using Morphologic Dating of Gully Incision

Yuval Shmilovitz[1,2], Eitan Shelef[3], Nimrod Wieler[1], Huiping Zhang[4], and Amit Mushkin[1]

[1]Geological Survey of Israel, Jerusalem, Israel, [2]The Fredy & Nadine Herrmann Institute of Earth Sciences, The Hebrew University of Jerusalem, Jerusalem, Israel, [3]Department of Geology and Environmental Science, University of Pittsburgh, Pittsburgh, PA, USA, [4]State Key Laboratory of Earthquake Dynamics, Institute of Geology, China Earthquake Administration, Beijing, China

Key Points:

- We proposed a morphologic approach for dating the abandonment of alluvial surfaces based on modeling gullies incised into them
- The proposed approach was successfully tested for multiple late Pleistocene surfaces in an arid study site in southern Israel
- The proposed modeling approach can help constrain changes in tectonic and climatic conditions for gully incision in both space and time

Supporting Information:

Supporting Information may be found in the online version of this article.

Correspondence to:

Y. Shmilovitz,
yuval.shmilovich@mail.huji.ac.il

Citation:

Shmilovitz, Y., Shelef, E., Wieler, N., Zhang, H., & Mushkin, A. (2023). Estimating the age of abandoned alluvial surfaces using morphologic dating of gully incision. *Journal of Geophysical Research: Earth Surface*, *128*, e2022JF006875. https://doi.org/10.1029/2022JF006875

Received 9 AUG 2022
Accepted 22 FEB 2023

Author Contributions:

Conceptualization: Yuval Shmilovitz, Eitan Shelef, Nimrod Wieler, Huiping Zhang, Amit Mushkin
Formal analysis: Yuval Shmilovitz
Funding acquisition: Huiping Zhang, Amit Mushkin
Investigation: Yuval Shmilovitz, Eitan Shelef, Nimrod Wieler, Huiping Zhang, Amit Mushkin
Methodology: Yuval Shmilovitz, Eitan Shelef, Nimrod Wieler, Amit Mushkin

Abstract The age of abandoned alluvial surfaces is a key component in quantifying landscape evolution processes, tectonic activity, and paleoclimate. However, limited resources, restricted field accessibility, lacking dating material and analytical constraints are often encountered when dating such landforms. To help mitigate these limitations, we propose a new and complementary surface dating approach that is based on calculating the duration of gully incision into a surface since its abandonment using a locally calibrated landscape evolution model. The approach consists of calibration of incision model parameters for abandoned alluvial surfaces with known age and then using the calibrated model to calculate the time required for gully profiles to form on nearby undated alluvial surfaces as a proxy for surface abandonment. The approach was tested on previously dated late Pleistocene (34 and 70 ka) alluvial terraces in the hyper-arid Negev desert (Israel). Calibrated model parameters were within the range reported for incision models in arid regions worldwide and late Pleistocene surface abandonment ages were recovered to within 10% accuracy. In contrast, modeled durations for gully incision into an older mid-Pleistocene surface previously dated to 230–549 ka were grossly underestimated at <120 ka. Field observations and approach tests indeed indicated that late Pleistocene model parameters should not be extrapolated as-is to model gully incision farther back through geologic time. Because the validity of the proposed ages depends on extrapolating the locally calibrated parameters of the incision model, we recommend that such dating be conducted with care and where assumptions will probably be valid.

Plain Language Summary An important feature for reconstructing paleoclimate and tectonic activity is determining the timing of when stream deposits were disconnected from the stream that deposited them to become abandoned alluvial surfaces. Here, we propose a new method for dating the abandonment of alluvial surfaces based on the age of gullies (erosional channels) incised into the surface after its abandonment as computed using a landscape evolution model. As a first step, the method requires calibration of the model parameters for a surface with an a priori known age. Based on the calibrated parameters, the model is then used to calculate the duration of the incision required to form observed gully profiles on nearby surfaces of unknown ages. The new approach was tested and successfully validated on previously dated alluvial surfaces in the Negev desert (Israel).

1. Introduction

Alluvial deposits and landforms record the response of Earth's landscape to changes in climate and tectonics over the Quaternary, and hence their dating is often used to study surface processes and to constrain rates of landscape evolution (Bull, 1991; Harvey et al., 1999; Malatesta et al., 2018; Tuzlak et al., 2022; Walk et al., 2020; Watchman & Twidale, 2002). Alluvial fans, for example, are widespread depositional landforms located along mountain fronts, where fluvial channels emerge from their mountainous catchments and transition to a less confined, lower-gradient flow regime that induces sediment deposition (Bull, 1991; Dimuth et al., 2020). Fan deposits are primarily comprised of relatively coarse-grained and poorly sorted sediments that aggrade episodically during mass-wasting or flood events (Blair & McPherson, 2009; Vincent et al., 2022). When alluvial deposits become disconnected from their upstream catchment, for example, due to flow diversion or down-cutting of the channel that transported them, they are commonly termed "abandoned" alluvial landforms. After abandonment and cessation of alluvial sedimentation, the dominant geomorphic processes on these abandoned alluvial landforms typically include weathering, soil development, and gully incision (e.g., Blair & McPherson, 2009; Greenbaum et al., 2020; McDonald et al., 2003).

Project Administration: Eitan Shelef, Amit Mushkin
Supervision: Eitan Shelef, Huiping Zhang, Amit Mushkin
Visualization: Eitan Shelef, Huiping Zhang, Amit Mushkin
Writing – original draft: Yuval Shmilovitz, Eitan Shelef, Amit Mushkin
Writing – review & editing: Yuval Shmilovitz, Eitan Shelef, Nimrod Wieler, Huiping Zhang, Amit Mushkin

In tectonically quiescent arid conditions, abandoned alluvial surfaces can persist for millions of years (e.g., Matmon et al., 2009), whereas in tectonically active or wetter conditions, incision processes ultimately degrade these landforms away (Bull, 1991). Because both the aggradation stages and degradation processes of alluvial landforms are sensitive to changes in discharge and tectonic activity, the timing of their abandonment is a pivotal component in studies that explore the transition between aggradational (depositional) to degradational (erosional) conditions in response to changes in climate (Amit et al., 2006; McDonald et al., 2003; Neagu et al., 2020; Owen et al., 1997; Ritter et al., 2000) as well as tectonics (Amit & Yaalon, 1996; Chen et al., 2018; Wells et al., 1988; Zielke et al., 2015).

Absolute dating of abandoned alluvial surfaces is most commonly achieved through "in situ" dating of the surface and near-surface deposits, with methodologies such as optically stimulated luminescence (OSL, e.g., Aitken, 1998; Gellman et al., 2018; Villacorta et al., 2019; Yu et al., 2019; Zinelabedin et al., 2022), cosmogenic radionuclides (CRN, e.g., Bierman & Turner, 1995; Liu et al., 1996; Matmon et al., 2003; Peri et al., 2022). While these methods provide key constraints on the landform age, their application is inherently spatially limited by cost, labor, accessibility of sampling sites, availability of suitable dating material, and/or analytical complexities in sample processing. Hence, "in situ" ages from a small number of dated sites are often extrapolated across large areas. Previous studies have focused on developing quantitative approaches for applying such extrapolations using regional empirical calibration curves between in situ surface ages and physical surface attributes that can be measured from remotely sensed data, such as spectroscopy (Crouvi et al., 2006), ground-based LiDAR (Mushkin et al., 2014), airborne LiDAR (Frankel & Dolan, 2007; Regmi et al., 2014), space-borne radar (Hetz et al., 2016) and imagery (D'Arcy et al., 2018).

"Morphologic dating," which typically builds on an optimized fit between measured and modeled topography of a geomorphic feature (Mayer, 1984; Nash, 1984), provides an additional complementary approach for estimating the age of abandoned alluvial surfaces. For example, Hsu and Pelletier (2004) showed that modeled duration of channel-bank diffusion in the southwest USA correlated well with the relative Pleistocene chronology of the abandoned alluvial surfaces hosting the gullies. Harkins and Kirby (2008) employed similar diffusion modeling concept to constrain the age of terrace risers and the tectonic slip rates they record along the Kunlun fault in China. In other settings, morphologic dating is also broadly utilized to constrain the timing of fault scarp formation (Amit et al., 1996; Andrews & Hanks, 1985; Hilley et al., 2010; Mayer, 1984; Nash, 1980; Pelletier et al., 2006), river profile development (Attal et al., 2011; Ferrier et al., 2013; Gran et al., 2013; Stock & Montgomery, 1999; Willett et al., 2014), and hillslope evolution processes (Lahusen et al., 2015; Petit et al., 2009; Roering, 2008). Accordingly, it appears that morphologic dating of abandoned alluvial surfaces, specifically in desert environments where landform preservation is commonly considered optimal, may benefit from recent advancements in the quality of topographic data and landscape evolution modeling (e.g., Temme et al., 2017).

Abandoned alluvial landforms in desert environments constitute a natural experiment of landscape evolution (Tucker, 2009) in which the external forcing (e.g., base-level change) and the initial condition (i.e., preincision topography) are relatively well constrained. In such settings, after the surface has been abandoned, an impervious layer of interlocking weathered clasts nested on a layer of aeolian dust (i.e., a "desert pavement") develops and smooths the initial bar-and-swale topography (e.g., Amit & Gerson, 1986). The progressively decreasing permeability and roughness of desert pavement surfaces can lead to increased discharge and fluvial shear stress in small rills that exceed the surface resistance to erosion during overland flow events, which in turn advances incision and formation of gullies (e.g., Greenbaum et al., 2020). The evolution of such ephemeral gullies is typically characterized by head-cut propagation during episodic and severe rainfall events (e.g., Shmilovitz et al., 2020), and is modulated by changes in the local base-level (commonly defined by the active channel that bounds the abandoned surface) (e.g., Wieler et al., 2022). The residual soil moisture in these dry landforms is relatively minor due to the low frequency of rainfall events and decreasing soil permeability through time (Greenbaum et al., 2020), and thus, its effect on overland flow processes and erosion is negligible in contrast to gullies in wetter environments that are commonly influenced by subsurface flow and "top-down" erosion processes (e.g., piping, Bernatek-Jakiel & Poesen, 2018).

Building on these well-studied and understood geomorphic trajectories of abandoned alluvial surfaces, we present a new geomorphic dating approach for alluvial surfaces that builds on process-based modeling of fluvial incision of channels (referred herein as "gullies") that internally drain abandoned alluvial surfaces. As desert pavement surfaces preserve the approximate (smoothed) elevation of the preincision topography of the abandoned landform (e.g.,

Greenbaum et al., 2020; Hetz et al., 2016; Mushkin et al., 2014), the initial preincision surface can be effectively reconstructed using topographic interpolations between preserved sections of desert pavement (Wieler et al., 2022). Consequently, the total magnitude of incision at each point along the present-day gully profile can be calculated as the elevation difference between the gully bed and the reconstructed preincision surface. This constraint on the magnitude of incision along a gully enables the use of a locally calibrated landscape evolution model to calculate the time required to form the observed gully profiles as a proxy for the abandonment age of the surface they incise.

2. Approach

The fundamental geomorphic assumptions at the base of the proposed surface dating approach are as follows: (a) The lag-time between the surface abandonment and the initiation of incision is negligible relative to the age of the surface and therefore the duration of gully incision calculated by the landscape evolution model can be used as a proxy for the abandonment age of the surface incised. Incipient gullies incised into ∼5 ka surfaces in the study area (see Section 3 below), and well-developed gullies on ∼30 ka surfaces suggest that the lag-time between surface abandonment and incision is indeed relatively short. (b) The total base-level lowering that the gully experienced during its evolution can be estimated as the elevation difference between the reconstructed, preincision surface and the gully bed at its outlet into the active channel (i.e., the channel that bounds the abandoned surface, (Wieler et al., 2022)). The preincision surface can be reconstructed using a linear topographic interpolation between preserved patches of desert pavement located on the surface of interest (e.g., van Gorp et al., 2015; Temme et al., 2017; Wieler et al., 2022, Section 4.2). Additional model assumptions depend on the geomorphologic transport function (GTF, Dietrich et al., 2003; Tucker & Hancock, 2010) that is used to describe the gully incision process. The GTF we used here was the stream power function (Howard, 1994; Whipple & Tucker, 1999) and hence we also assumed that: (c) The distribution of drainage areas along each gully has remained approximately constant since the time of surface abandonment (e.g., Attal et al., 2011), (d) Gully incision into the alluvial deposit is primarily a detachment-limited process (i.e., incision is limited by the flow's ability to detach material from the bed) that can be formulated using the stream power equation commonly used to describe bedrock incision (Howard, 1994; Whipple & Tucker, 1999). These assumptions are supported by field observations in the study area (Section 4.3.1). An additional and fundamental working assumption employed is that the locally calibrated model parameters (e.g., erodibility coefficient that reflects the resistance of the surface to erosion. See Section 4.3.2 below) are applicable across time and space to the landforms we seek to date. In addition to field observations, internal consistency tests for the modeling results (Section 4.3.4) were used to evaluate the validity of these assumptions.

The proposed dating approach consists of 3 main stages (Figure 1). (a) Establishment of a morphostratigraphic alluvial landform framework for the study site and acquisition of high-resolution topographic data; (b) Gully selection and setup of initial and boundary conditions for the landscape evolution model, for example, delineation of gully profiles, their catchments, and preincision surface based on the preserved desert pavement on the surface of interest; (c) Model application: *Step I—Local calibration* of the incision-model parameters using the topography of multiple gullies that incise an abandoned surface with an a priori known age; *Step II—Model inversion* in which the calibrated incision model is used to compute the duration of the incision required to form observed gully profiles on nearby "target" alluvial surfaces of unknown age (hereafter "target surfaces").

3. Study Site

We tested the proposed approach in a hyperarid study site located in the southern Negev desert, along the southern segment of the Dead Sea Transform (Garfunkel et al., 1981) within the Arava valley in southern Israel (Figure 2). The region is a warm desert (subzero temperatures are rarely reached) with a mean annual rainfall of <30 mm (Israel Meteorological Service, http://www.ims.gov.il). Most rainfall occurs between October and May during discrete, high-intensity rainstorm events associated with high interannual and intra-annual variability (Sharon & Kutiel, 1986). The alluvial surfaces studied are part of the Shehoret fan, which has an upstream catchment area of ∼28 km^2 that drains from ∼west to east into the Arava valley (Figure 2). As the ephemeral Shehoret stream exits its mountainous catchment, it transitions into a gravelly alluvial fan with deposits that dip slightly to the east, subparallel to the active stream. The alluvial deposits are comprised of carbonate and magmatic clasts and form a set of abandoned Pleistocene-Holocene terraces (e.g., Gellman et al., 2018) that are typically covered by desert pavements (Amit et al., 1993) with gradually decreasing clast size with terrace age (Mushkin et al., 2014). Vegetation cover is sparse and occurs mainly within the gullies that incise the abandoned surfaces and the active

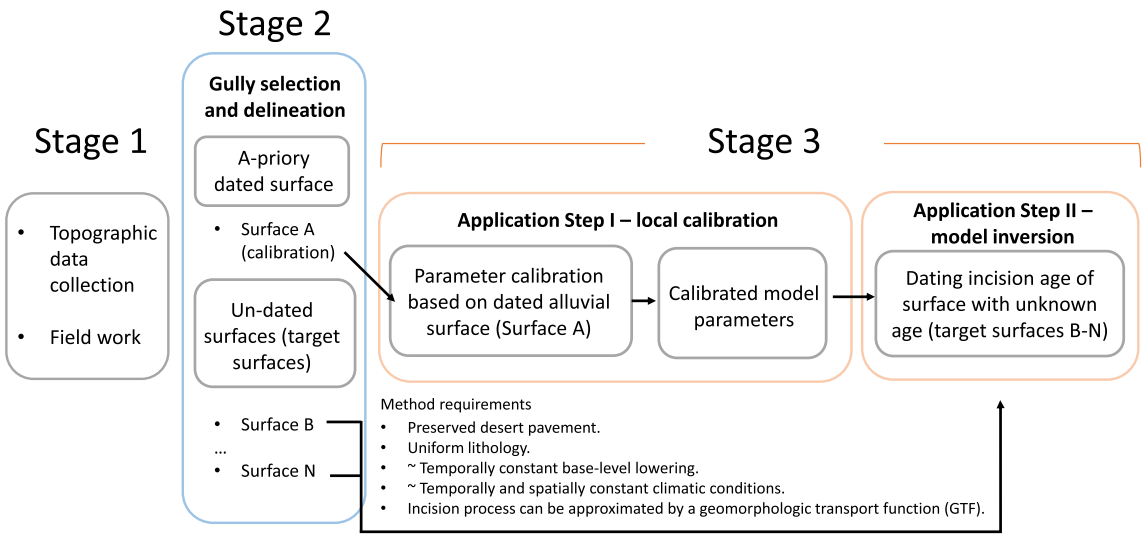

Figure 1. Geomorphic dating of abandoned alluvial surfaces—method flow chart. Stage 1: Field work and establishment of a morphostratigraphic framework. Acquisition of high-resolution topographic data. Stage 2: Gully selection and delineation. Stage 3: Model application—Step I: calibration of the incision model parameters based on the topography of multiple gullies incised into a surface with a known age. Step II: Inversion of the calibrated model to compute the incision duration of multiple gullies on target surfaces.

channels that bound these surfaces. The reg soils developed on abandoned alluvial surfaces in this region are up to ~200 cm in depth and are characterized by an accumulation of salts (gypsum and halite), mainly in their C horizon (Amit & Gerson, 1986). The absence of a calcic horizon in the reg soils of this region suggests that the mean precipitation and vegetation cover have remained low and roughly constant since the early Pleistocene (Amit et al., 2006), supporting our assumptions about constant erosion parameters in time and space.

Six main generations of alluvial terraces were previously mapped and dated in the Shehoret fan: Qa01 (549 ± 133 ka), Qa02 (230–549 ka), Qa1 (70 ± 6 ka), Qa2 (34 ± 3 ka), Qa3 (14 ± 2 ka), and Qa4 (4.6 ± 0.7 ka) (numbers represent average ages and standard deviations, Gellman et al. (2018); Porat et al. (2010), Figures 2 and

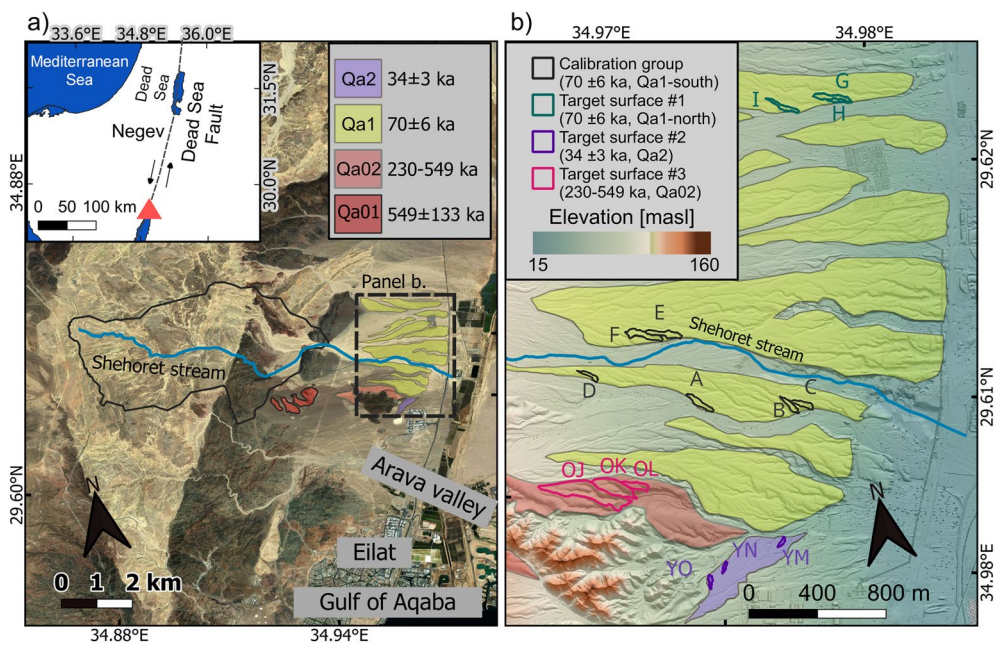

Figure 2. Study area. (a) Satellite image overlay with a generalized morphostratigraphic map for the Shehoret fan terraces. Inset—location of the study site (red triangle) ~10 km north of the Gulf of Aqaba and the city of Eilat. (b) Hillshade map of the Shehoret terraces examined in the present study.

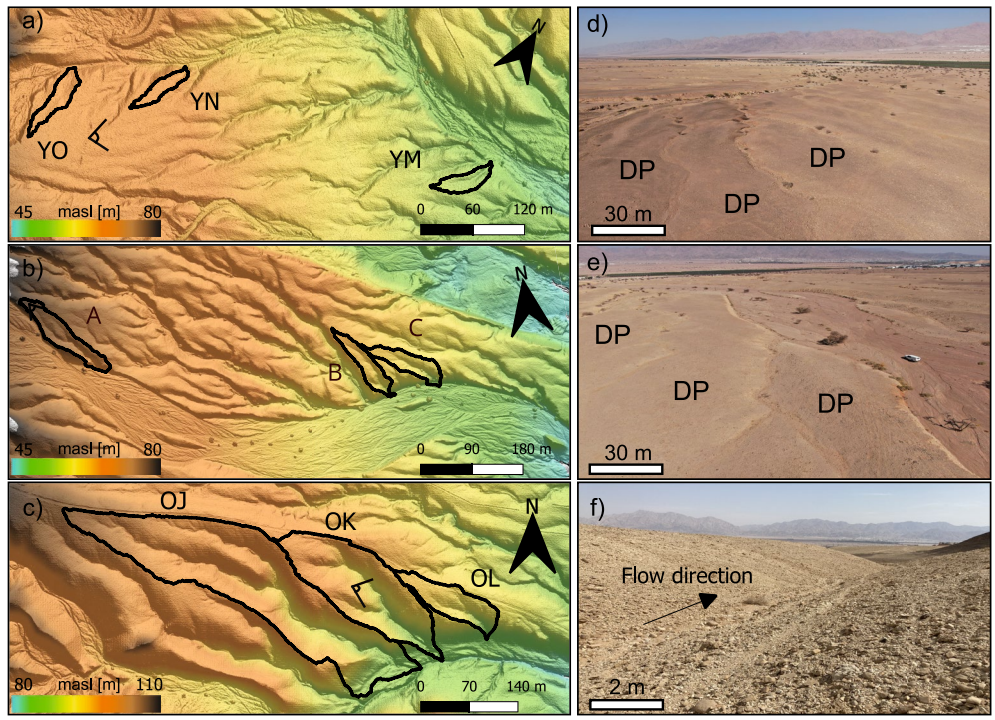

Figure 3. Gullies incised into abandoned alluvial surfaces in the Shehoret alluvial fan (the locations are shown in Figure 2). (a–c) Hillshade maps based on LiDAR-derived DEMs for Qa2 (34 ± 3 ka), Qa1-south (70 ± 6 ka), and Qa02 (230–549 ka). Black triangles in a, b, and c mark the viewpoint of the corresponding drone, satellite, and field pictures shown in panels d, e, and f, respectively. DP refers to preserved surfaces covered by desert pavement that separate gully drainages from one another and are used for reconstructing the preincision surface. Examples of the match between the reconstructed preincision surfaces and the preserved gully divides are shown in Figure S2 in Supporting Information S1.

3 (Qa3 and Qa4 are not shown)). Tectonic tilting that initiated in the mid-Pleistocene caused a progressive reorganization of regional flow patterns (Gellman et al., 2018), such that while terraces Qa01, Qa02, Qa1, Qa3, and Qa4 contain mostly carbonate clasts, Qa2 located in the southern parts of the fan has an ~ equal proportion of carbonate and magmatic clasts. North-south striking normal faults associated with the Dead Sea Transform dissect the eastern parts of the Shehoret fan with a vertical throw that decreases northwards and accounts for ~6 m base-level drop for Qa1 in the southern parts of the fan (Qa1-south) and ~2 m of base-level drop for Qa1 in the northern parts of the fan (Qa1-north) (Enzel et al., 1996). Mature desert pavements and well-developed gullies characterize the surfaces of Qa2, Qa1, and Qa02 (Figure 3). Incipient gullies are observed in the downstream sections of the Qa3 and Qa4 surfaces (Figure 4 in Porat et al. (2010)). While the banks of the gullies incising late Pleistocene terraces Qa2 and Qa1 typically intersect the terrace surfaces at fairly sharp angles, the banks of the gullies incising the mid-Pleistocene Qa01 typically grade into the terrace surface and form more "rounded" cross-sections (Figure S1 in Supporting Information S1). In addition, the profiles of gullies incised in Qa1 and Qa2 are generally smooth, whereas the profiles of gullies incised in Qa02 are characterized by fluctuations in channel gradients.

4. Methodology

4.1. Fieldwork and Topographic Data

The morphostratigraphic framework for the Shehoret terraces used in the present study builds on a wealth of previous studies conducted at this site that focused on reg soil development (e.g., Amit et al., 1993), rock weathering, surface evolution (e.g., Mushkin et al., 2014), surface dating (Hetz et al., 2016; Porat et al., 2010) and tectonic geomorphology (Amit et al., 1996; Enzel et al., 1996). Fieldwork in the present study was focused on the characterization of the desert pavement surfaces and detailed surveys of the gullies that incise them. Topographic analyses were based on a 0.5 m pixel^{-1} Digital Elevation Model (DEM) covering terraces Qa1-4 (Figure 2). The DEM was derived from airborne LiDAR data acquired at an average point density of 4 pts m^{-2}, an absolute vertical accuracy of ±0.15 m, and geo-referencing uncertainty of ±1.0 m. Vertical precision in the DEM was estimated at ±0.05 m.

4.2. Gully Selection Criteria and Model Initial and Boundary Conditions

Gully delineation was performed on the DEM. We selected overall 14 gullies, developed on one Qa02 surface, two Qa1 surfaces, and one Qa2 surface (Figure 2). The criteria for gully selection were as follows: (a) the gully catchment is minimally truncated by active channels (as these may indicate changes in catchment area) and (b) the upper gully catchment is not channelized, as this may imply that this upper part used to have a larger catchment area. We used a D8 flow routing algorithm (using TopoToolbox MATLAB add-on functions (Schwanghart & Scherler, 2014)) to delineate the basins and longitudinal profiles of active gullies. To conservatively identify preserved surfaces in each gully basin, we queried DEM pixels of ungullied alluvial surfaces (hereafter termed "preserved surface pixels") to be identified based on the drainage area threshold (<10 m^2) and distance from the gully outlets (within 10% of the maximal Euclidean distances from the outlet). We then visually inspected these surfaces on the high-resolution DEM to test and validate this automated procedure. By applying these conditions, eroded divide sections, which are more common toward the outlet of the basin, are not considered preserved surface pixels. To approximate the initial preincision topography of the alluvial surface into which the gully is incised, we fit a plane (two-dimensional linear regression) to the preserved surface pixels (see the preserved surface area separating gullies watersheds in Figure 3) and projected it over the entire gully drainage. The fitted planes in each drainage generally match isolated sections of preserved surfaces along the downstream portion of the gully's present divide (Figure S2 in Supporting Information S1). The initial, preincision topography of each gully was estimated from the profile of the reconstructed surface following the route of the present gully.

We assumed that gully incision into abandoned alluvial surfaces was controlled by the downcutting the active channel that bounds the abandoned surface and acts as a local base level. The total incision of the bounding channel was measured as the elevation difference between the reconstructed preincision surface and the present elevation at the gully outlet, where it drains into the bounding channel. Accordingly, in each simulation, we inferred the downcutting rate of the bounding channel by dividing the total incision by the prescribed simulation duration, with the implicit assumption that this rate is constant over time.

4.3. Model Application

4.3.1. Erosion Model

The gullies in the study area are characterized by a "v-shaped" cross-sectional profile, steep cut banks, areas with slope fluctuations (potentially indicative of knickpoints and/or reflecting head-cuts), thin sediment cover on their channel bed (Figure 3 and Figures S3–S7 in Supporting Information S1), and therefore likely evolved through a detachment limited incision process into the cohesive alluvium that underlies the abandoned surface (i.e., erosion rate controlled by the detachment rate of the cohesive alluvium). Given these characteristics, the GTF selected to simulate channel incision at Shehoret was the stream-power model (Howard, 1994; Whipple & Tucker, 1999):

$$E = KA^m S^n \tag{1}$$

where E [L T^{-1}] is the erosion rate, K [L^{1-2m} T^{-1}] is a measure of incision efficiency (Lague, 2014) that depends on lithology, climate, and channel geometry, A [L^2] is the upstream drainage area, S [L L^{-1}] is the topographic slopes, and m and n are exponents that acknowledge that the erosion rate may be a nonlinear function of A and S, respectively. For simplicity, to minimize the number of parameters used for calibration and modeling, we assume that diffusive processes within the channels are negligible, such that incision can be modeled by Equation 1 alone. We acknowledge that as the surface smoothens, its permeability and roughness decrease and thus the potential for runoff generation and gully incision may increase (Greenbaum et al., 2020; S. Wells et al., 2014; Yair & Klein, 1973; Yair & Lavee, 1976), yet, for simplicity, we assume that the hydrologic and lithologic characteristics of the surface remain constant through time. Likewise, we recognize that the initial surface morphology is likely divergent (i.e., distributary). However, we implicitly assume that convergent topography (i.e., dendritic, Bowman, 2018) forms soon after surface abandonment and that once it is established, the distribution of drainage areas (A) along the gully remained approximately constant through time and can be mapped from the present-day topography (Ferrier et al., 2013; Stock & Montgomery, 1999).

Channel erodibility, K, and the exponents, m and n, were determined using the calibration procedure described in Section 4.3.2 below. For each time step, the elevation at each model node relative to the model boundary was updated by the following equation:

$$\frac{\partial z}{\partial t} = U - E, \tag{2}$$

where z [L] is elevation, t [T] is time and U [L T^{-1}] is the uplift rate. Note that U is relative to the base level (i.e., the bounding channel at the outlet of the gully), and therefore its magnitude is equivalent to the aforementioned downcutting rate of the bounding channel. The model integrates Equation 2 through time using a fourth-to fifth-order explicit Runge–Kutta integration with time-stepping constrained by the Courant criteria (Press et al., 1992).

4.3.2. Step I—Model Calibration

To locally determine model parameters, K, m, and n (Equation 1), we used an inversion scheme that optimizes the fit between the simulated and observed gully topography on a "calibration" terrace, that is, a terrace with an a priori known age. Calibration was obtained through a comparison between the modeled and observed topography of the gully profiles, a common calibration procedure in studies that utilize landscape evolution models (e.g., Attal et al., 2011; Gran et al., 2013; Temme et al., 2017). The comparison relies on an objective function that transforms the elevation differences between modeled and simulated profiles into a scalar (RMSD):

$$\mathrm{RMSD} = \sqrt{\frac{\sum_{i=1}^{n}\left(z_{\mathrm{obs},i} - z_{\mathrm{sim},i}\right)^2}{n}}, \tag{3}$$

where $z_{(\mathrm{obs},i)}$ and $z_{(\mathrm{sim},i)}$ are the observed and simulated gully elevations, respectively, n is the number of DEM pixels (and model nodes) along with the gully profile, and i is the node/pixel index.

The calibration procedure we employed utilizes a two-tier procedure to approximate a global minimum (optimum) in the objective function (Equation 3) and the K, m, and n values associated with it. The base-level lowering, U, at the model boundary (the outlet of the gully) is set to the elevation difference between the initial and current topography at the gully outlet, divided by the age of the surface, which is known a priori only for the calibration surface. The model was executed iteratively, over a period constrained by the surface age, to find the combinations of K, m, and n that minimize the RMSD value. To identify parameter combinations associated with a global rather than a local minimum of the objective function (Equation 3), we used a sequential optimization method where first, a grid-search calibration is performed on a large parameter space to identify the area (within the parameter space) around the global minimum. Then, within this space and starting with a given random initial parameter combination, we iteratively search for the parameter combination that minimizes the RMSD (i.e., moving within the parameter space toward the area with lower RMSD) through a Nelder-Mead search algorithm (also known as downhill simplex method, Lagarias et al. (2006)). This method is based on a direct search comparison of the objective function (e.g., RMSD) and is commonly applied to nonlinear optimization problems. Because the resulting parameter combination may be sensitive to the initial choice of parameter combination, this search was repeated 100 times wherein each iteration the initial parameter combination is randomly selected (assuming uniform distribution) from the parameter space identified by the global grid-search. To account for uncertainty, the iterations that produced the lowest 2% of RMSD values (out of the aforementioned 100 iterations) were considered feasible parameter combinations (e.g., Shmilovitz et al., 2020). To account for the general pattern of all gullies and avoid overfitting to a specific gully, the calibration was performed based on the mean of the RMSD values for all the gullies in the calibration surface (see below). Such "grouped" calibration accounts for the general pattern of all gullies and avoids overfitting to a specific gully profile. All calculations were based on MATLAB's simplex search-based optimization technique implemented through the fminsearch tool.

A subset of six gullies incised into Qa1-south (70 ± 6 ka, gullies A-F, Figures 2 and 3) were used for "grouped" calibration of the model parameters (i.e., Section 4.3.1). The grid-search calibration was performed for m and n ranging between 0.1 and 0.6, and 1–2.1, respectively, based on values presented by Harel et al. (2016) and references therein. For K, we first performed a few trial-and-error estimations to narrow the range to 10^{-5}–10^{-3} $\left[\mathrm{m}^{1-2m}\ \mathrm{year}^{-1}\right]$, which is within the reported range of K in arid regions (Harel et al., 2016 and references therein).

4.3.3. Step II—Determining the Age of Target Alluvial Surfaces

The calibrated model parameters from step I were used in a landscape evolution model (Equation 1) to calculate the duration of incision that best predicts observed gully profiles on nearby target surfaces of unknown age. Three gullies were examined for each target surface to ensure internal consistency and to reduce bias from a given gully selection. First, the initial, preincision topography of the target surfaces was computed as described in Section 4.2. Then, using the calibrated parameters, the model was iteratively executed for different time-spans (i.e., duration of incision), starting with the approximated initial conditions. In each iteration, U is defined based on the prescribed model time-span and the observed elevation difference between the initial surface and the gully

outlet into the channel that bounds the abandoned fan. The objective function was used (Equation 3) to find the time-span that optimizes the fit between the observed and simulated gully profiles. To evaluate the range of feasible surface-ages, we repeated this procedure for all feasible parameter combinations (i.e., the aforementioned combinations that produced the best 2% of all RMSD values) for each of the simulated gullies.

The model parameters calibrated on surface Qa1-south (70 ± 6 ka, Section 5.2) were applied to calculate incision duration for the following: (a) Three gullies incised into surface Qa1-north (G, H, and I, 70 ± 6 ka); (b) Three gullies incised into surface Qa2 (YO, YM, and YN, 34 ± 3 ka), and (c) Three gullies incised into surface Qa02 (OJ, OL, and OK, 230–549 ka). The previously determined ages for surfaces Qa1-north, Qa2, and Qa02 were not used as model inputs but were rather used as independent validation data for the model results.

4.3.4. Testing the Calibration Procedure and Internal Consistency Tests

To robustly evaluate the performance of the proposed dating approach, we tested (a) whether the calibration procedure succeeds in recovering the prescribed parameters, (b) whether the "group" calibration (Section 4.3.2) is internally consistent, and (c) whether the calibrated model parameters vary with the surface chosen for calibration. In the first test, we executed the calibration procedure in a fully controlled setting in which synthetic gully profiles were simulated over 70 ka using Equation 2, prescribed initial conditions, and an arbitrary set of preselected model parameters K, m, and n. We then applied the calibration procedure, using a simulation duration of 70 ka, to test how well the calibration procedure based on the optimal RMSD recovers the preselected model parameters that were used to simulate the synthetic gully profiles. In the second test, we used the calibrated parameter combinations based on the 'group' calibration of gullies A-F (Section 4.3.2) to compute the incision duration for each of these gullies separately. An internally consistent system is expected to produce similar ages for all these gullies. In the third test, we applied the calibration procedure separately for: (a) three gullies incised into the Qa1-north surface (G, H, and I, 70 ± 6 ka) where the abandoned surface is elevated by approximately 2 m above the bounding channel (in contrast with Qa1-south where the abandoned surface is elevated by approximately 6 m above the bounding channel) and, (b) three gullies incised into the Qa2 surface (YM, YN, and YO, 34 ± 3 ka) where the abandoned surface is elevated by approximately 2 m above the bounding channel, and (c) three gullies incised into the Qa02 terrace (OJ, OK, and OL, 230–549 ka) here the abandoned surface is elevated by approximately 10 m above the bounding channel (Figure S1 in Supporting Information S1). A setting where climate and erodibility are homogeneous in space and time is expected to generate similar calibrated parameters for all surfaces.

5. Results

5.1. Model Calibration at Shehoret

The calibration procedure results on Qa1-south gullies helped quantify the model sensitivity to variability in K [m^{1-2m} $year^{-1}$] and the ratio m/n (Figure 4a). The best RMSD error was 0.26 [m] (Figure 4b), and the parameter combinations that are within 2% of the best-fit RMSD are $1.06*10^{-4}$ ($+1.64*10^{-4}$, $-5.5*10^{-5}$), 0.48 (+0.07, −0.1) and 1.65 (+0.11, −0.06), for K [m^{1-2m} $year^{-1}$], m, and n respectively (results are presented as the optimal value, followed by the maximum and minimum values of all feasible combinations, Table 1, Figure 4). The ratio m/n in all feasible parameter combinations ranged between 0.22 and 0.34.

5.2. Modeled Incision Duration and Surface Ages at Shehoret

Computed incision durations (Figure 6a) for gullies G, H, and I, on the Qa1-north surface, were 77 (+5, −5) ka, 66 (+5, −3) ka, 68 (+9, −4) ka, respectively. RMSD values ranged between 0.09 and 0.11[m] and the mean modeled incision duration for the three gullies was 70 (+6, −4) ka (within 10% of the independently obtained surface-ages for the terrace (70 ± 6 ka). The computed incision ages for gullies YM, YN, and YO, incised into the Qa2 surface were 39 (+6, −5) ka, 33 (+11, −8) ka, and 36 (+8, −6) ka, respectively. RMSD values ranged between 0.11–0.21 [m] and the resulting mean incision duration calculated for the three gullies was 37 (+9, −7) ka (within 10% of the independently obtained surface-ages for these terrace (34 ± 3 ka)). Computed incision durations for gullies OJ, OK, and OL, incised on the Qa02 surface were 116 (+27, −31) ka, 118 (+14, −16) ka, and 55 (+6, −3) ka, respectively. RMSD values ranged between 0.37–0.43 [m] and the resulting mean incision duration calculated for the three gullies was 97 (+15.7, −16.7) ka. Overall, incision durations calculated for the gullies incised on the Qa1-north and Qa2 surfaces were tightly clustered within 20% of the independently obtained surface-ages for these terraces (Figure 6). Incision durations calculated for the gullies incising the Qa02 surface were more scattered and significantly younger than the independently obtained surface-age for this terrace.

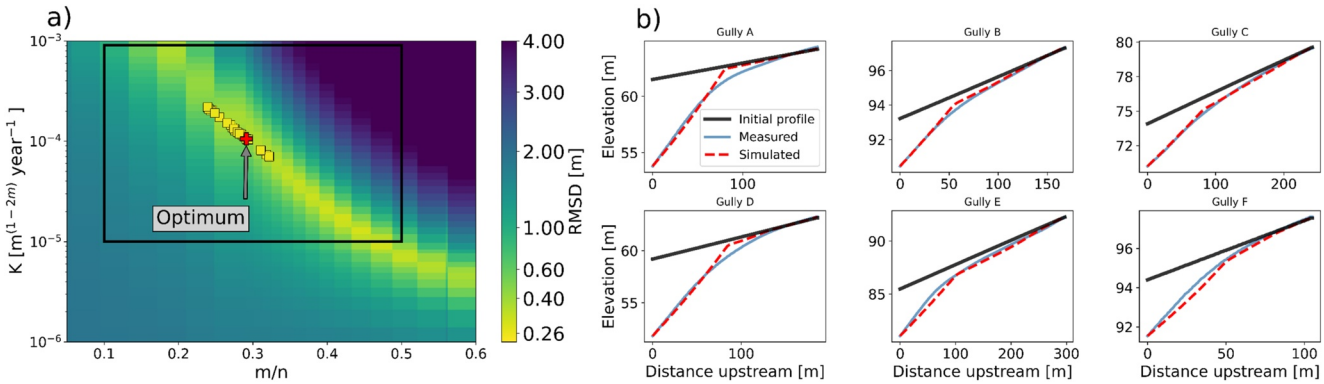

Figure 4. Model calibration. (a) A "solution" surface describing changes in the value of the objective function (RMSD) with changes in K and m/n space for 70 ± 6 ka gullies used for calibration (in surface Qa1-south in Figure 1). The black rectangle indicates the parameter space in which the local calibration was performed. The yellow squares represent endpoints of local calibration iterations that are within 2% of the minimal RMSD (optimum, red cross). (b) Measured (blue lines) versus simulated (red lines) and initial (black lines) gully profiles using the best-fit parameter set calibrated based on gullies A-F (*K*, *m*, and *n* of 1.06*10–4, 0.48, and 1.65, respectively).

5.3. Internal Consistency and Calibration Tests

The test of the calibration procedure shows that the recovered model parameters for the synthetic gully profiles (Section 4.3.4) were identical to the parameters used to generate them, indicating that from an analytical standpoint, the calibration procedure can accurately recover the stream power parameters *K*, *m*, and *n* (Equation 1). The test of internal consistency between gullies within the same surface shows that the separately calculated incision durations for each of the gullies used for the 'group-calibration' (gullies A-F) (Section 4.3.2) are within 10% of each other, indicating that the group-calibrated parameters are consistent with the topography of all these gullies (Figure S8 in Supporting Information S1). The test of consistency in calibrated model parameters between surfaces shows that calibration based on surfaces Qa1-north and Qa2 produces model parameters that were comparable to those of the calibration surface (i.e., Qa1-south), whereas model parameters calibrated for the Qa02 terrace were different (Table 1, Figure 5, test 3).

6. Discussion

6.1. Method Performance

Incision durations were calculated separately for each of the gullies examined on the late Pleistocene Qa1-north and Qa2 surfaces using the model parameters calibrated based on the Qa1-south surface (Sections 5.1 and 5.2). All these gully "incision ages" were tightly clustered and concordant (within 20%) with independently determined surface-ages for the respective terraces they incise (Figure 6), which in turn supports the fundamental assumption that calculated incision duration from the model can be used as a proxy for surface age. Furthermore, these results indicate that model parameters calibrated on a given surface of a known age can be spatially extrapolated to effectively model gully incision on other nearby abandoned alluvial surfaces that have a different composition and may have experienced different tectonic conditions. For example, Qa2 comprises an equal proportion of carbonate and magmatic clasts, while the surface used for calibration (Qa1-south) is predominately composed of carbonate clasts, yet the model parameters calibrated based on Qa1-south yielded a Qa2 age that is within 10% of the a priori

Table 1
Calibrated Parameters for Different Calibration Groups

			K [m^{1-2m} year^{-1}]			m			n			m/n		
Terrace-age [ka]	Terrace ID	Terrace ID	Min	Max	Optimum	Min	Max	Optimum	Min	Max	Optimum	Min	Max	Optimum
70 ± 6	Qa1-south	0.26	5E−5	2.7E−4	1E−4	0.38	0.55	0.48	1.59	1.76	1.65	0.22	0.35	0.29
70 ± 6	Qa1-south	0.13	6E−5	6E−5	6E−5	0.6	0.6	0.6	1.8	1.8	1.8	0.33	0.33	0.33
34 ± 3	Qa2	0.09	8E−5	5E−4	1.4E−4	0.52	0.60	0.59	1.82	2.22	1.97	0.24	0.32	0.30
230–549	Qa02	0.77	2E−6	3E−6	3E−6	0.58	0.62	0.59	1.00	1.11	1.02	0.55	0.59	0.58

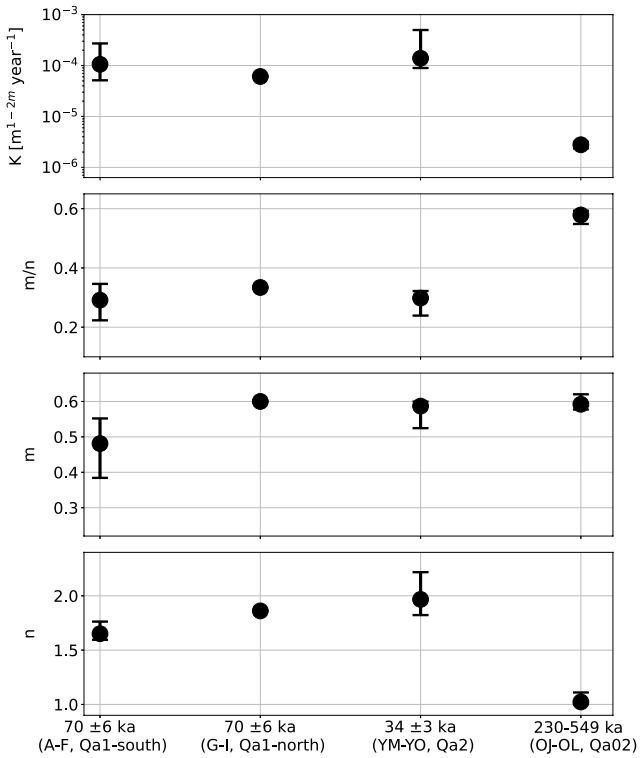

Figure 5. Calibrated model parameters based on sets of gullies from surfaces of different ages. Dots show the calibrated best-fit parameters and whiskers the minimum-maximum range for the feasible calibrated parameter (2% of the minimal RMSD).

known age (according to the mean calculated incision duration of the three gullies in Qa2 group). Similarly, Qa1-north experienced ∼2 m of tectonically induced uplift (i.e., lowering of the bounding channel) over a period of about 70 ka, while the Qa1-south calibration surface experienced ∼6 m of such uplift over the same period, yet the model parameters calibrated based on the Qa1-south surface enabled accurate dating of the Qa1-north surface (within 10% of the a priori known age according to the mean calculated incision duration of the three gullies in the Qa1-north group). In addition, the success in dating, as well as in calibration and internal consistency tests (Section 5.3) support the model assumptions, some of which are difficult to validate (i.e., the assumptions regarding short lag-time between surface abandonment and incision, and temporally constant drainage area distribution). While fully validating these assumptions will require further investigation, it appears that for the purpose of dating, the simplifying assumptions we make lead to reasonable results.

The success in dating surfaces Qa1-north and Qa2 with model parameters calibrated based on Qa1-south suggests that parameters calibrated based on the Qa1-north (70 ± 6 ka) or Qa2 (34 ± 3 ka) surfaces will be similar to those calibrated based on the Qa1-south surface (70 ± 6 ka). Indeed, K and m/n values calibrated based on these three surfaces are similar (Figure 5, Table 1). Overall, the results based on Qa1-south, Qa1-north, and Qa2 indicate that the proposed morphologic dating method produces ages that are consistent with independently determined ages obtained using other methods, and that the calibrated parameters are similar between abandoned surfaces of different ages and/or tectonic offset. This suggests that alluvial surfaces of unknown ages can be dated via geomorphic dating of gully incision based on locally calibrated model parameters. However, applying this methodology to date the nearby Qa02 surface (independently dated to 230–549 ka) yielded significantly younger ages (116 (+27, −31) ka, 118 (+14, −16) ka, and 55 (+6, −3)

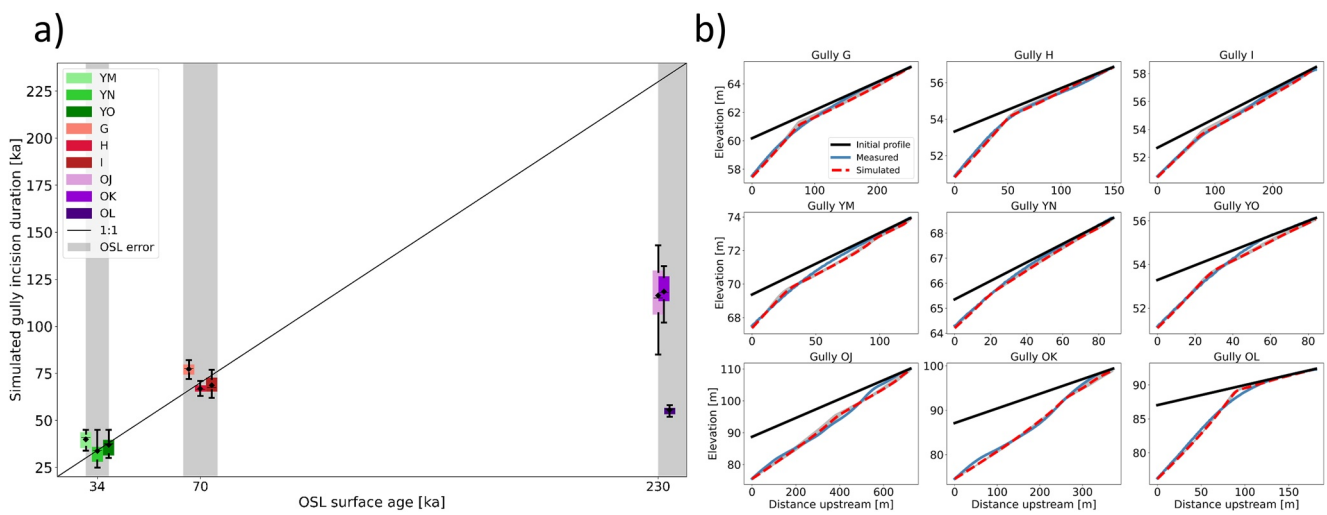

Figure 6. Surface dating via geomorphic dating of gully incision. (a) The Gray shaded area represents the uncertainty in the optically stimulated luminescence (OSL) ages (x-axis only). Each boxplot represents the calculated age distribution per gully (boxes are slightly offset for clarity). In each box plot, the black dot represents the mean, horizontal lines represent the median, the colored area is bounded between the 25 and 75 percentiles and the whisker represents the minima and maxima of feasible values. The black line shows 1:1 relation between OSL surface age and morphologically dated gully incision duration. (b) Measured (blue line), simulated (red line) and initial (black line) gully profiles based on the best-fit parameter set. The gray-shaded area around the red lines marks the distribution of profiles for all feasible parameter sets (note that each profile is an end-of-simulation profile using one of the calibrated parameter sets over the time that provides the best-fit to the measured profile).

ka, for gullies OJ, OK, and OL, respectively). Thus, it appears that extrapolation of the proposed dating method back in time beyond the age of the calibration surface should be taken with caution.

6.2. Mid-Pleistocene Terrace (Qa02)

To examine the disagreement between gully incision ages on the Qa02 surface (118, 116, 55 ka) and its independently obtained surface-age (230–549 ka), we calibrated K, m, and n values based on gullies OJ, OK, and OL, assuming a minimum surface-age of 230 ka. We found that K was an order of magnitude lower and m/n was ∼twice higher than those calibrated based on Qa1-south, Qa1-north, and Qa2 (Figure 5, Table 1, Figures S9–S11 in Supporting Information S1). Lower K values for Qa02 compared to Qa1 and Qa2 are also produced when the values of m and n are held constant across all surfaces (Figure S12 in Supporting Information S1). The relatively low K value for Qa02 explains the younger incision age obtained for the gullies incising this surface when using model parameters that were calibrated to the late Pleistocene (70 ± 6 ka) Qa1-south surface (gullies A-F).

Qa02 is topographically distinct from all other surfaces, which may point to changes in tectonic or climatic conditions that violate the assumptions of temporally uniform K, m, n, and base-level lowering rate (Sections 2). These characteristics include the rounded surface of Qa02 compared to the flatter surface of Qa1 and Qa2 (Figure S1 in Supporting Information S1), a feature that questions the preservation of the initial, preincision surface topography and suggests that it was modified by hillslope processes. Furthermore, the presence of slope fluctuations along the gullies OJ and OK incised into the Qa02 surface relative to other surfaces (Figure 6b and Figures S3–S7 in Supporting Information S1) may reflect temporal variations in the base-level lowering rate and/or variations in lithologic composition. In addition to these topographic characteristics, the distinctively broad range of inversed incision ages between gullies in the Qa02 surface (i.e., 118, 116, 55 ka) compared to all other surfaces also hints at the complex evolution of this surface (Section 5.2).

The possibility of temporal changes in the base-level lowering rate for Qa02 is supported by the findings of Gellman et al. (2018), who recognized a shift in the direction of fluvial flows in the Shehoret drainage in the late Pleistocene–Holocene and attributed it to regional northward tilting. This tilting could increase the mean base-level lowering of the Qa1 (70 ± 6 ka) surface compared to that of the Qa02 (230–549 ka) surface. Such an increased base-level lowering rate would violate the assumption of a temporally constant base-level lowering rate that underlies the proposed morphologic dating and could conceivably explain the morphologically young gully profiles in Qa02. A possible hint for such complexity may be observed in gullies OJ and OK (Figure 6b), which have a higher RMSD (Section 5.2) and are characterized by fluctuations in slope along with the gully profile (Figure 6 and Figure S7 in Supporting Information S1), which may represent knickpoints of different ages formed through temporal changes in base-level lowering rate.

Alternatively, the mismatch between calculated gully incision durations and the surface age of Qa02 may reflect a change in the hydro-climatic settings and possibly erosion rates between the abandonment of Qa1 at 70 ± 6 ka and Qa02 at 230 ka, leading to changes in erosion parameters (Whipple & Tucker, 1999). In the southern Negev, studies have proposed an increase in extreme storm and flood magnitudes during the Last-Glacial-Maximum (Enzel et al., 2012; Yokochi et al., 2019). An increase in the storm intensities after ∼70 ka, would potentially increase the storm erosion efficiency and the frequency of erosive events (Dunkerley, 2018; Shmilovitz et al., 2020; Wang et al., 2016) which can explain the higher calibrated K value based on the gullies incised into Qa1 (70 ± 6 ka) and Qa2 (34 ± 3 ka) compared to the ones incised into Qa02 (230–549 ka) surface (Figure 5, Table 1). Changes in frequency-magnitude relations of extreme rainstorms were previously suggested to trigger alterations between incision and deposition phases in arid areas, impacting alluvial and colluvial landforms (Boroda et al., 2011; Enzel et al., 2003, 2012; McCarroll et al., 2021; Miller et al., 2010).

In addition to climatic and tectonic changes, differences in surface and soil characteristics may cause a mismatch between modeled and OSL-based ages of the gullies incised into the Qa02 surfaces. Differences in surface clast size can cause a mismatch in the modeled surface age, as clast size affects erosion threshold on dryland slopes. Mushkin et al. (2014) have shown that surface clast size on these surfaces decreases during the first ∼50 ka, asymptotically reaching a ∼constant value after 100 ka. However, the proposed method succeeds in dating the Qa2 surface (34 ± 3 ka, when clast size is rapidly changing with time) based on parameters calibrated on the Qa1 surface (70 ± 6 ka, when clast size approaches a constant value), but fails to date the Qa02 surface (>230 ka, when clast size is approximately constant). Thus, we conclude that clast size does not meaningfully affect the method's

results. Differences between Pleistocene and Holocene Reg soils can cause different erosion rates. Pleistocene reg soil in the study area is characterized by a pronounced accumulation of secondary gypsum and a thicker salt layer compared to the Holocene soils (Boroda et al., 2011). Such gypsum and salt can increase soil cementation and thus cause a time-varying erosion rate, which can explain the lower calibrated K values we obtain for Qa02 relative to Qa1 and Qa2 (Figure 5). The presence of more resistant horizons in the reg soil of older surfaces could also cause comparably large fluctuations in the slope along gullies incised into Qa02 (Figure S3–S7 in Supporting Information S1). The unsuccessful dating of Qa02 may also be explained by temporal variations in vegetation cover. However, as these alluvial surfaces are not covered by vegetation under current conditions and were probably not covered by vegetation since the Pleistocene (Amit et al., 2006), changes in vegetation cover are unlikely to cause this mismatch in age.

Attempting to determine the exact conditions under which the gullies of the Shehoret fan have developed is beyond the scope of this study. Nonetheless, the pronounced differences in the values of calibrated parameters between Qa02 and the younger surfaces, together with the proposed climatic and tectonic changes in this region, suggest that recovering incision model parameters for a priori dated surfaces (Figure 5) can potentially help detect temporal or spatial changes in tectonic and/or climatic conditions.

6.3. What can we Learn From the Calibrated Model Parameters?

The theoretical development of the stream power concept argues that the concavity index (i.e., *m/n*) should typically range between 0.35 and 0.6 (Tucker & Whipple, 2002), which is higher than the range of values computed in this study (calibrated *m/n* values range between 0.22 and 0.34, Figure 5, Table 1). However, large-scale compilations (Chen et al., 2019; Harel et al., 2016) indicate that lower *m/n* values (e.g., 0.2–0.3) can occur in arid areas such as the Shehoret catchment. In such hyper-arid settings, low *m/n* values may reflect a hydrological regime in which overland flow events are rare and spatially discontinuous, and sediment is mobilized primarily during extreme events (Whipple & Tucker, 1999). The calibrated *K* and *m/n* values reported here are also aligned with the values reported by Harel et al. (2016) for arid areas. This may reflect the low vegetation cover and the higher likelihood of rainfall events that diverge from mean conditions (Marra et al., 2021; Marra & Morin, 2015, 2018), as well as high erosion efficiency (Dunkerley, 2019; Wolman & Miller, 1960; Yue et al., 2020). The calibrated *n* values, which were greater than 1, may support the notion that incision and sediment transport in these areas are threshold controlled and may depend on the stochastic distribution of rainstorms and floods (Adams et al., 2020; Lague, 2014).

6.4. Limitations of the Proposed Dating Method

In the examples for successful dating of surfaces shown here (Figure 6), the proposed surface dating approach uses Equation 1 as the geomorphic transport function (GTF) that describes gully incision. This selection implies that gully incision is primarily detachment limited and that the contribution of transport-limited or threshold-controlled erosional processes is negligible. Whereas Equation 1 is widely used in fluvial geomorphology and its predictions are often consistent with empirical findings (Darling et al., 2020; Lague, 2014), it is unlikely to capture the full complexity of the natural incision and sediment transport process (Baynes et al., 2020; Venditti et al., 2020). Yet, despite the relative simplicity of the approach we propose and its underlying assumptions, its success in reproducing the gully profiles (i.e., low RMSD values relative to the relief of gully profile), and in constraining the age of the Qa1-north (70 $\pm$ 6 ka) and Qa2 (34 $\pm$ 3 ka) surfaces (Figure 6), suggests that it relies on a reasonable approximation for the conditions and processes under which the analyzed gullies are incised.

An important part of the proposed method is the calibration of model parameters. Given the potential sensitivity of these parameters to changes in climate and soil characteristics (i.e., Section 6.2), the proposed method is most suitable in settings where these characteristics remain approximately constant over the approximate age of dated features. Although this is a major limitation of the proposed approach, in settings where these conditions hold, dating can be accomplished over large spatial scales and a variety of abandoned alluvial surfaces, at a relatively low cost and effort.

The proposed method can be strengthened by addressing some of these simplified assumptions in future work. For instance, including erosion and deposition under transport-limited conditions (e.g., Gasparini et al., 2007; Hobley et al., 2011), as well as a streamflow variability and GTFs that account for a threshold for channel erosion

may better describe the natural process forming these gullies, resulting in improved age constraints as recent studies pointed to the significant influence of hydrological processes on the erosion patterns over a long time scale (Barnhart et al., 2020; Deal et al., 2018). However, we note that using such GTFs will require calibration of additional model parameters that may increase uncertainties and computation time. Likewise, assigning different erodibility coefficients to different soil and alluvial horizons and including additional (if existed) erosion processes (e.g., bank failures and "top-down"piping) may also improve the accuracy of the method.

7. Conclusions

This study presents a new method for dating alluvial surfaces that is based on an inverse modeling approach that calculates the time required to obtain gully profiles that match the observed profiles of gullies incised into abandoned alluvial surfaces. The dating method uses the stream power function as the geomorphologic transport function (GTF) utilized to simulate the temporal evolution of the gully profiles. Model parameters need to be calibrated based on gully profiles from an independently dated surface and can then be used to compute gully incision ages on nearby abandoned surfaces with unknown ages. We tested the method on a set of the previously dated mid to late Pleistocene terraces in southern Israel. The model parameters were calibrated based on gullies incised into a 70 ± 6 ka terrace. Using the calibrated parameters, we computed surface-ages of 70 (+6, –4) ka and 37 (+9, –4) ka for neighboring alluvial terraces of diverse lithologic composition and base-level lowering rates that were previously dated to 70 (±6), and 34 (±3) ka, respectively. However, when attempting to use model parameters calibrated on a 70 (±6) ka terrace to date an older terrace, where field observations indicated that the method's underlying assumptions were violated, the proposed method yielded significantly younger incision ages of 97 (+15.7, −16.7) ka than the independently dated age of this surface (230–549 ka). We conclude that the proposed modeling approach can be used to effectively date alluvial surfaces at a regional scale as long as the method's underlying assumptions are met.

Data Availability Statement

We used the open-source TopoToolBox 2 MATLAB software (Schwanghart & Scherler, 2014) for topographic analysis. The functions used for the proposed method application are available at: https://github.com/yuvalsmilo/GullyIncisionOnAlluvialSurface.git.

Acknowledgments
This study was partially funded by an ISF grant (Grant 2568/17 to AM), Hewlett International Grant Program for ES, and a fellowship to YS from the Hebrew University Advanced School for Environmental Studies.

References

Adams, B. A., Whipple, K. X., Forte, A. M., Heimsath, A. M., & Hodges, K. V. (2020). Climate controls on erosion in tectonically active landscapes. *Science Advances*, *6*(42). https://doi.org/10.1126/sciadv.aaz3166

Aitken, M. J. (1998). *Introduction to optical dating: The dating of quaternary sediments by the use of photon-stimulated luminescence*. Clarendon Press.

Amit, R., Enzel, Y., & Sharon, D. (2006). Permanent quaternary hyperaridity in the Negev, Israel, resulting from regional tectonics blocking Mediterranean frontal systems. *Geology*, *34*(6), 509–512. https://doi.org/10.1130/G22354.1

Amit, R., & Gerson, R. (1986). The evolution of Holocene Reg (gravelly) soils in deserts. An example from the Dead Sea region. *Catena*, *13*(1–2), 59–79. https://doi.org/10.1016/S0341-8162(86)80005-4

Amit, R., Gerson, R., Yaalon, D. H., & Yaalon, D. H. (1993). Stages and rate of the gravel shattering process by salts in desert Reg soils. *Geoderma*, *57*(3), 295–324. https://doi.org/10.1016/0016-7061(93)90011-9

Amit, R., Harrison, J. B. J., Enzel, Y., & Porat, N. (1996). Soils as a tool for estimating ages of quaternary fault scarps in a hyperarid environment—The southern Arava valley, the Dead Sea rift, Israel. *Catena*, *28*(1–2), 21–45. https://doi.org/10.1016/S0341-8162(96)00028-8

Amit, R., & Yaalon, D. H. (1996). The micromorphology of gypsum and halite in Reg soils—The Negev desert, Israel. *Earth Surface Processes and Landforms*, *21*(12), 1127–1143. https://doi.org/10.1002/(SICI)1096-9837(199612)21:12<1127::AID-ESP656>3.0.CO;2-G

Andrews, D. J., & Hanks, T. C. (1985). Scarp degraded by linear diffusion: Inverse solution for age. *Journal of Geophysical Research*, *90*(B12), 10193. https://doi.org/10.1029/JB090iB12p10193

Attal, M., Cowie, P. A., Whittaker, A. C., Hobley, D., Tucker, G. E., & Roberts, G. P. (2011). Testing fluvial erosion models using the transient response of Bedrock Rivers to tectonic forcing in the Apennines, Italy. *Journal of Geophysical Research*, *116*(2), 2005. https://doi.org/10.1029/2010JF001875

Barnhart, K. R., Tucker, G. E., Doty, S. G., Shobe, C. M., Glade, R. C., Rossi, M. W., & Hill, M. C. (2020). Inverting topography for landscape evolution model process representation: 3. Determining parameter ranges for select mature geomorphic transport laws and connecting changes in fluvial erodibility to changes in climate. *Journal of Geophysical Research: Earth Surface*, *125*(7), e2019JF005287. https://doi.org/10.1029/2019JF005287

Baynes, E. R. C., Lague, D., Steer, P., Bonnet, S., & Illien, L. (2020). Sediment flux-driven channel geometry adjustment of bedrock and mixed gravel–bedrock rivers. *Earth Surface Processes and Landforms*, *45*(14), 3714–3731. https://doi.org/10.1002/ESP.4996

Bernatek-Jakiel, A., & Poesen, J. (2018). Subsurface erosion by soil piping: Significance and research needs. *Earth-Science Reviews*, *185*, 1107–1128. https://doi.org/10.1016/j.earscirev.2018.08.006

Bierman, P., & Turner, J. (1995). 10Be and 26Al evidence for exceptionally low rates of Australian bedrock erosion and the likely existence of pre-pleistocene landscapes. *Quaternary Research*, *44*(3), 378–382. https://doi.org/10.1006/qres.1995.1082

Blair, T. C., & McPherson, J. G. (2009). Processes and forms of alluvial fans. In *Geomorphology of desert environments* (pp. 413–467). Springer Netherlands. https://doi.org/10.1007/978-1-4020-5719-9_14

Boroda, R., Amit, R., Matmon, A., ASTER Team, Finkel, R., Porat, N., et al. (2011). Quaternary-scale evolution of sequences of talus flatirons in the hyperarid Negev. *Geomorphology*, *127*(1–2), 41–52. https://doi.org/10.1016/j.geomorph.2010.12.003

Bowman, D. (2018). Principles of alluvial fan morphology. *Principles of Alluvial Fan Morphology*. https://doi.org/10.1007/978-94-024-1558-2

Bull, W. B. (1991). *Geomorphic response to climatic change*. Oxford University Press.

Chen, S. A., Michaelides, K., Grieve, S. W. D., & Singer, M. B. (2019). Aridity is expressed in river topography globally. *Nature*, *573*(7775), 573–577. https://doi.org/10.1038/s41586-019-1558-8

Chen, T., Liu-Zeng, J., Shao, Y., Zhang, P., Oskin, M. E., Lei, Q., & Li, Z. (2018). Geomorphic offsets along the creeping Laohu Shan section of the Haiyuan fault, northern Tibetan Plateau. *Geosphere*, *14*(3), 1165–1186. https://doi.org/10.1130/GES01561.1

Crouvi, O., Ben-Dor, E., Beyth, M., Avigad, D., & Amit, R. (2006). Quantitative mapping of arid alluvial fan surfaces using field spectrometer and hyperspectral remote sensing. *Remote Sensing of Environment*, *104*(1), 103–117. https://doi.org/10.1016/J.RSE.2006.05.004

D'Arcy, M., Mason, P. J., Roda-Boluda, D. C., Whittaker, A. C., Lewis, J. M. T., & Najorka, J. (2018). Alluvial fan surface ages recorded by Landsat-8 imagery in Owens Valley, California. *Remote Sensing of Environment*, *216*, 401–414. https://doi.org/10.1016/J.RSE.2018.07.013

Darling, A., Whipple, K., Bierman, P., Clarke, B., & Heimsath, A. (2020). Resistant rock layers amplify cosmogenically-determined erosion rates. *Earth Surface Processes and Landforms*, *45*(2), 312–330. https://doi.org/10.1002/ESP.4730

Deal, E., Braun, J., & Botter, G. (2018). Understanding the role of rainfall and hydrology in determining fluvial erosion efficiency. *Journal of Geophysical Research: Earth Surface*, *123*(4), 744–778. https://doi.org/10.1002/2017JF004393

Dietrich, W. E., Bellugi, D. G., Sklar, L. S., Stock, J. D., Heimsath, A. M., & Roering, J. J. (2003). Geomorphic transport laws for predicting landscape form and dynamics. *Geophysical Monograph Series*, *135*, 103–132. https://doi.org/10.1029/135GM09

Dimuth, W. D., Welivitiya, P., Willgoose, G. R., & Hancock, G. R. (2020). Geomorphological evolution and sediment stratigraphy of numerically simulated alluvial fans. https://doi.org/10.1002/esp.4872

Dunkerley, D. (2018). How is overland flow produced under intermittent rain? An analysis using plot-scale rainfall simulation on dryland soils. *Journal of Hydrology*, *556*, 119–130. https://doi.org/10.1016/J.JHYDROL.2017.11.003

Dunkerley, D. (2019). Rainfall intensity bursts and the erosion of soils: An analysis highlighting the need for high temporal resolution rainfall data for research under current and future climates. *Earth Surface Dynamics*, *7*(2), 345–360. https://doi.org/10.5194/esurf-7-345-2019

Enzel, Y., Amit, R., Grodek, T., Ayalon, A., Lekach, J., Porat, N., et al. (2012). Late Quaternary weathering, erosion, and deposition in Nahal Yael, Israel: An "impact of climatic change on an arid watershed". *Bulletin of the Geological Society of America*, *124*(5–6), 705–722. https://doi.org/10.1130/B30538.1

Enzel, Y., Amit, R., Porat, N., Zilberman, E., & Harrison, B. J. (1996). Estimating the ages of fault scarps in the Arava, Israel. *Tectonophysics*, *253*(3–4), 305–317. https://doi.org/10.1016/0040-1951(95)00072-0

Enzel, Y., Bookman, R., Sharon, D., Gvirtzman, H., Dayan, U., Ziv, B., & Stein, M. (2003). Late Holocene climates of the Near East deduced from Dead Sea level variations and modern regional winter rainfall. *Quaternary Research*, *60*(3), 263–273. https://doi.org/10.1016/j.yqres.2003.07.011

Ferrier, K. L., Huppert, K. L., & Perron, J. T. (2013). Climatic control of bedrock river incision. *Nature*, *496*(7444), 206–209. https://doi.org/10.1038/nature11982

Frankel, K. L., & Dolan, J. F. (2007). Characterizing arid region alluvial fan surface roughness with airborne laser swath mapping digital topographic data. *Journal of Geophysical Research*, *112*(F2), 2025. https://doi.org/10.1029/2006JF000644

Garfunkel, Z., Zak, I., & Freund, R. (1981). Active faulting in the Dead Sea rift. *Tectonophysics*, *80*(1–4), 1–26. https://doi.org/10.1016/0040-1951(81)90139-6

Gasparini, N. M., Whipple, K. X., & Bras, R. L. (2007). Predictions of steady state and transient landscape morphology using sediment-flux-dependent river incision models. *Journal of Geophysical Research*, *112*(F3), F03S09. https://doi.org/10.1029/2006JF000567

Gellman, Y., Matmon, A., Mushkin, A., & Porat, N. (2018). Drainage system reorganization and late quaternary tectonic deformation along the southern Dead Sea Transform. *Quaternary Research*, *90*(2), 380–393. https://doi.org/10.1017/qua.2018.53

Gran, K. B., Finnegan, N., Johnson, A. L., Belmont, P., Wittkop, C., & Rittenour, T. (2013). Landscape evolution, valley excavation, and terrace development following abrupt postglacial base-level fall. *Bulletin of the Geological Society of America*, *125*(11–12), 1851–1864. https://doi.org/10.1130/B30772.1

Greenbaum, N., Mushkin, A., Porat, N., & Amit, R. (2020). Runoff generation, rill erosion and time-scales for hyper-arid abandoned alluvial surfaces, the Negev desert, Israel. *Geomorphology*, *358*, 107101. https://doi.org/10.1016/j.geomorph.2020.107101

Harel, M.-A., Mudd, S. M., & Attal, M. (2016). Global analysis of the stream power law parameters based on worldwide 10Be denudation rates. *Geomorphology*, *268*, 184–196. https://doi.org/10.1016/j.geomorph.2016.05.035

Harkins, N., & Kirby, E. (2008). Fluvial terrace riser degradation and determination of slip rates on strike-slip faults: An example from the Kunlun fault, China. *Geophysical Research Letters*, *35*(5), L05406. https://doi.org/10.1029/2007GL033073

Harvey, A. M., Wigand, P. E., & Wells, S. G. (1999). Response of alluvial fan systems to the late Pleistocene to Holocene climatic transition: Contrasts between the margins of pluvial Lakes Lahontan and Mojave, Nevada and California, USA. *Catena*, *36*(4), 255–281. https://doi.org/10.1016/S0341-8162(99)00049-1

Hetz, G., Mushkin, A., Blumberg, D. G., Baer, G., & Ginat, H. (2016). Estimating the age of desert alluvial surfaces with spaceborne radar data. *Remote Sensing of Environment*, *184*, 288–301. https://doi.org/10.1016/j.rse.2016.07.006

Hilley, G. E., Delong, S., Prentice, C., Blisniuk, K., & Arrowsmith, J. R. (2010). Morphologic dating of fault scarps using airborne laser swath mapping (ALSM) data. *Geophysical Research Letters*, *37*(4), 0–5. https://doi.org/10.1029/2009GL042044

Hobley, D. E. J., Sinclair, H. D., Mudd, S. M., & Cowie, P. A. (2011). Field calibration of sediment flux dependent river incision. *Journal of Geophysical Research*, *116*(4), 1–18. https://doi.org/10.1029/2010JF001935

Howard, A. D. (1994). A detachment limited model of drainage basin evolution. *Water Resources Research*, *30*(7), 2261–2285. https://doi.org/10.1029/94WR00757

Hsu, L., & Pelletier, J. D. (2004). Correlation and dating of Quaternary alluvial-fan surfaces using scarp diffusion. *Geomorphology*, *60*(3–4), 319–335. https://doi.org/10.1016/j.geomorph.2003.08.007

Lagarias, J. C., Reeds, J. A., Wright, M. H., & Wright, P. E. (2006). Convergence properties of the Nelder—Mead simplex method in low dimensions. *SIAM Journal on Optimization*, *9*(1), 112–147. https://doi.org/10.1137/S1052623496303470

Lague, D. (2014). The stream power river incision model: Evidence, theory and beyond. *Earth Surface Processes and Landforms*, *39*(1), 38–61. https://doi.org/10.1002/esp.3462

Lahusen, S. R., Duvall, A. R., Booth, A. M., & Montgomery, D. R. (2015). Surface roughness dating of long-runout landslides near Oso, Washington (USA), reveals persistent postglacial hillslope instability. *Geology*, *44*(2), 111–114. https://doi.org/10.1130/G37267.1

Liu, B., Phillips, F. M., Pohl, M. M., & Sharma, P. (1996). An alluvial surface chronology based on cosmogenic 36Cl dating, Ajo mountains (Organ pipe cactus National Monument), southern Arizona. *Quaternary Research*, *45*(1), 30–37. https://doi.org/10.1006/qres.1996.0003

Malatesta, L. C., Avouac, J. P., Brown, N. D., Breitenbach, S. F. M., Pan, J., Chevalier, M. L., et al. (2018). Lag and mixing during sediment transfer across the Tian Shan piedmont caused by climate-driven aggradation–incision cycles. *Basin Research*, *30*(4), 613–635. https://doi.org/10.1111/BRE.12267

Marra, F., Armon, M., Adam, O., Zoccatelli, D., Gazal, O., Garfinkel, C. I., et al. (2021). Toward narrowing uncertainty in future projections of local extreme precipitation. *Geophysical Research Letters*, *48*(5), e2020GL091823. https://doi.org/10.1029/2020GL091823

Marra, F., & Morin, E. (2015). Use of radar QPE for the derivation of intensity-duration-frequency curves in a range of climatic regimes. *Journal of Hydrology*, *531*, 427–440. https://doi.org/10.1016/j.jhydrol.2015.08.064

Marra, F., & Morin, E. (2018). Autocorrelation structure of convective rainfall in semiarid-arid climate derived from high-resolution X-Band radar estimates. *Atmospheric Research*, *200*, 126–138. https://doi.org/10.1016/j.atmosres.2017.09.020

Matmon, A., Simhai, O., Amit, R., Haviv, I., Porat, N., McDonald, E., et al. (2009). Desert pavement-coated surfaces in extreme deserts present the longest-lived landforms on Earth. *Bulletin of the Geological Society of America*, *121*(5–6), 688–697. https://doi.org/10.1130/B26422.1

Matmon, A., Bierman, P. R., Larsen, J., Southworth, S., Pavich, M., & Caffee, M. (2003). Temporally and spatially uniform rates of erosion in the southern Appalachian Great Smoky Mountains. *Geology*, *31*(2), 155–158. https://doi.org/10.1130/0091-7613(2003)031<0155:tasuro>2.0.co;2

Mayer, L. (1984). Dating quaternary fault scarps formed in alluvium using morphologic parameters. *Quaternary Research*, *22*(3), 300–313. https://doi.org/10.1016/0033-5894(84)90024-3

McCarroll, N. R., Pederson, J. L., Hidy, A. J., & Rittenour, T. M. (2021). Chronostratigraphy of talus flatirons and piedmont alluvium along the Book Cliffs, Utah—Testing models of dryland escarpment evolution. *Quaternary Science Reviews*, *274*, 107286. https://doi.org/10.1016/j.quascirev.2021.107286

McDonald, E. V., McFadden, L. D., Wells, S. G., Enzel, Y., & Lancaster, N. (2003). *Regional response of alluvial fans to the Pleistocene-Holocene climatic transition, Mojave Desert, California* (pp. 189–206). Special Papers-Geological Society of America.

Miller, D. M., Schmidt, K. M., Mahan, S. A., McGeehin, J. P., Owen, L. A., Barron, J. A., et al. (2010). Holocene landscape response to seasonality of storms in the Mojave Desert. *Quaternary International*, *215*(1–2), 45–61. https://doi.org/10.1016/j.quaint.2009.10.001

Mushkin, A., Sagy, A., Trabelci, E., Amit, R., & Porat, N. (2014). Measuring the time and scale-dependency of subaerial rock weathering rates over geologic time scales with ground-based lidar. *Geology*, *42*(12), 1063–1066. https://doi.org/10.1130/G35866.1

Nash, D. B. (1980). Morphologic dating of degraded normal fault SCARPS1.

Nash, D. B. (1984). Morphologic dating of fluvial terrace scarps and fault scarps near West Yellowstone, Montana. *The Geological Society of America Bulletin*, *95*(12), 1413–1424. https://doi.org/10.1130/0016-7606(1984)95<1413:MDOFTS>2.0.CO;2

Neagu, N., Matmon, A., Enzel, Y., & Porat, N. (2020). Quaternary evolution of a hyperarid drainage under climatic fluctuations and rift-margin base-level fall, NE Negev, Israel. *Geomorphology*, *354*, 107042. https://doi.org/10.1016/j.geomorph.2020.107042

Owen, L. A., Windley, B. F., Cunningham, W. D., Badamgarav, J., & Dorjnamjaa, D. (1997). Quaternary alluvial fans in the Gobi of southern Mongolia: Evidence for neotectonics and climate change. *Journal of Quaternary Science*, *12*(3), 239–252. https://doi.org/10.1002/(sici)1099-1417(199705/06)12:3<239::aid-jqs293>3.0.co;2-p

Pelletier, J. D., DeLong, S. B., Al-Suwaidi, A. H., Cline, M., Lewis, Y., Psillas, J. L., & Yanites, B. (2006). Evolution of the Bonneville shoreline scarp in west-central Utah: Comparison of scarp-analysis methods and implications for the diffusions model of hillslope evolution. *Geomorphology*, *74*(1–4), 257–270. https://doi.org/10.1016/j.geomorph.2005.08.008

Peri, V. G., Haghipour, N., Christl, M., Terrizzano, C., Kaveh-Firouz, A., Leiva, M. F., et al. (2022). Quaternary landscape evolution in the Western Argentine Precordillera constrained by 10Be cosmogenic dating. *Geomorphology*, *396*, 107984. https://doi.org/10.1016/J.GEOMORPH.2021.107984

Petit, C., Gunnell, Y., Gonga-Saholiariliva, N., Meyer, B., & Séguinot, J. (2009). Faceted spurs at normal fault scarps: Insights from numerical modeling. *Journal of Geophysical Research*, *114*(B5), 5403. https://doi.org/10.1029/2008JB005955

Porat, N., Amit, R., Enzel, Y., Zilberman, E., Avni, Y., Ginat, H., & Gluck, D. (2010). Abandonment ages of alluvial landforms in the hyperarid Negev determined by luminescence dating. *Journal of Arid Environments*, *74*(7), 861–869. https://doi.org/10.1016/j.jaridenv.2009.10.018

Press, W. H., Teukolsky, S. A., Vetterling, W. T., & Flannery, B. P. (1992). Numerical recipes in C. Citeseer.

Regmi, N. R., Mcdonald, E. V., & Bacon, S. N. (2014). Mapping Quaternary alluvial fans in the southwestern United States based on multiparameter surface roughness of lidar topographic data. *Journal of Geophysical Research: Earth Surface*, *119*(1), 12–27. https://doi.org/10.1002/2012JF002711

Ritter, J. B., Miller, J. R., & Husek-Wulforst, J. (2000). Environmental controls on the evolution of alluvial fans in Buena Vista Valley, North Central Nevada, during late quaternary time. *Geomorphology*, *36*(1–2), 63–87. https://doi.org/10.1016/S0169-555X(00)00048-9

Roering, J. J. (2008). How well can hillslope evolution models "explain" topography? Simulating soil transport and production with high-resolution topographic data. *Bulletin of the Geological Society of America*, *120*(9–10), 1248–1262. https://doi.org/10.1130/B26283.1

Schwanghart, W., & Scherler, D. (2014). Short communication: TopoToolbox 2-MATLAB-based software for topographic analysis and modeling in Earth surface sciences. *Earth Surface Dynamics*, *2*, 1–7. https://doi.org/10.5194/esurf-2-1-2014

Sharon, D., & Kutiel, H. (1986). The distribution of rainfall intensity in Israel, its regional and seasonal variations and its climatological evaluation. *Journal of Climatology*, *6*(3), 277–291. https://doi.org/10.1002/JOC.3370060304

Shmilovitz, Y., Morin, E., Rinat, Y., Haviv, I., Carmi, G., Mushkin, A., & Enzel, Y. (2020). Linking frequency of rainstorms, runoff generation and sediment transport across hyperarid talus-pediment slopes. *Earth Surface Processes and Landforms*, *45*(7), 1644–1659. https://doi.org/10.1002/esp.4836

Stock, J. D., & Montgomery, D. R. (1999). Geologic constraints on bedrock river incision using the stream power law. *Journal of Geophysical Research*, *104*(B3), 4983–4993. https://doi.org/10.1029/98jb02139

Temme, A. J. A. M., Armitage, J., Attal, M., van Gorp, W., Coulthard, T. J., & Schoorl, J. M. (2017). Developing, choosing and using landscape evolution models to inform field-based landscape reconstruction studies. *Earth Surface Processes and Landforms*, *42*(13), 2167–2183. https://doi.org/10.1002/esp.4162

Tucker, G. E. (2009). Natural experiments in landscape evolution. *Earth Surface Processes and Landforms*, *34*(10), 1450–1460. https://doi.org/10.1002/esp.1833

Tucker, G. E., & Hancock, G. R. (2010). Modelling landscape evolution. *Earth Surface Processes and Landforms*, *35*(1), 28–50. https://doi.org/10.1002/esp.1952

Tucker, G. E., & Whipple, K. X. (2002). Topographic outcomes predicted by stream erosion models: Sensitivity analysis and intermodel comparison. *Journal of Geophysical Research*, *107*(B9), ETG1-1–ETG1-16. https://doi.org/10.1029/2001jb000162

Tuzlak, D., Pederson, J., Bufe, A., & Rittenour, T. (2022). Patterns of incision and deformation on the southern flank of the Yellowstone hotspot from terraces and topography. *GSA Bulletin*, *134*(5–6), 1319–1333. https://doi.org/10.1130/B35923.1

van Gorp, W., Temme, A. J. A. M., Veldkamp, A., & Schoorl, J. M. (2015). Modelling long-term (300ka) upland catchment response to multiple lava damming events. *Earth Surface Processes and Landforms*, *40*(7), 888–900. https://doi.org/10.1002/esp.3689

Venditti, J. G., Li, T., Deal, E., Dingle, E., & Church, M. (2020). Struggles with stream power: Connecting theory across scales. *Geomorphology*, *366*, 106817. https://doi.org/10.1016/J.GEOMORPH.2019.07.004

Villacorta, S. P., Evans, K. G., De Torres, T. J., Llorente, M., & Prendes, N.-N. (2019). Geomorphological evolution of the Rimac River's alluvial fan, Lima. *Peru*, *23*(3), 409–424. https://doi.org/10.1007/s12303-018-0049-5

Vincent, L. T., Eaton, B. C., Leenman, A. S., & Jakob, M. (2022). Secondary geomorphic processes and their influence on alluvial fan morphology, channel behavior and flood hazards. *Journal of Geophysical Research: Earth Surface*, *127*(2), e2021JF006371. https://doi.org/10.1029/2021JF006371

Walk, J., Stauch, G., Reyers, M., Vásquez, P., Sepúlveda, F. A., Bartz, M., et al. (2020). Gradients in climate, geology, and topography affecting coastal alluvial fan morphodynamics in hyperarid regions—The Atacama perspective. *Global and Planetary Change*, *185*, 102994. https://doi.org/10.1016/J.GLOPLACHA.2019.102994

Wang, W., Yin, S., Xie, Y., Liu, B., & Liu, Y. (2016). Effects of four storm patterns on soil loss from five soils under natural rainfall. *Catena*, *141*, 56–65. https://doi.org/10.1016/j.catena.2016.02.019

Watchman, A. L., & Twidale, C. R. (2002). Relative and "absolute" dating of land surfaces. *Earth-Science Reviews*, *58*(1–2), 1–49. https://doi.org/10.1016/S0012-8252(01)00080-0

Wells, S., McFadden, L. D., McDonald, E. V., Eppes, M. C., Young, M. H., & Wood, Y. A. (2014). Desert pavement process and form: Modes and scales of landscape stability and instability in arid regions. In *EGU general assembly conference abstracts* (p. 8060).

Wells, S. G., Bullard, T. F., Menges, C. M., Drake, P. G., Karas, P. A., Kelson, K. I., et al. (1988). Regional variations in tectonic geomorphology along a segmented convergent plate boundary Pacific coast of Costa Rica. *Geomorphology*, *1*(3), 239–265. https://doi.org/10.1016/0169-555X(88)90016-5

Whipple, K. X., & Tucker, G. E. (1999). Dynamics of the stream-power river incision model: Implications for height limits of mountain ranges, landscape response timescales, and research needs. *Journal of Geophysical Research*, *104*(B8), 17661–17674. https://doi.org/10.1029/1999JB900120

Wieler, N., Mushkin, A., Zhang, H., Sagy, A., Porat, N., Shmilovitz, Y., et al. (2022). Geomorphic dating of across-fault gully incision reveals time-invariant late quaternary slip-rates at the eastern termination of the Altyn Tagh fault. *Geophysical Research Letters*, *49*(8). https://doi.org/10.1029/2021GL096933

Willett, S. D., McCoy, S. W., Taylor Perron, J., Goren, L., & Chen, C. Y. (2014). Dynamic reorganization of river basins. *Science*, *343*(6175). https://doi.org/10.1126/science.1248765

Wolman, M. G., & Miller, J. P. (1960). Magnitude and frequency of forces in geomorphic processes. *The Journal of Geology*, *68*(1), 54–74. https://doi.org/10.1086/626637

Yair, A., & Klein, M. (1973). The influences of surface properties on flow and erosion processes on debris covered slopes in an arid area. *Catena*, *1*, 1–18. https://doi.org/10.1016/s0341-8162(73)80002-5

Yair, A., & Lavee, H. (1976). Runoff generative process and runoff yield from arid talus mantled slopes. *Earth Surface Processes*, *1*(3), 235–247. Retrieved from http://onlinelibrary.wiley.com/doi/10.1002/esp.3290010305/abstract

Yokochi, R., Ram, R., Zappala, J. C., Jiang, W., Adar, E., Bernier, R., et al. (2019). Radiokrypton unveils dual moisture sources of a deep desert aquifer. *Proceedings of the National Academy of Sciences of the United States of America*, *116*(33), 16222–16227. https://doi.org/10.1073/pnas.1904260116

Yu, S. Y., Du, J., Hou, Z., Shen, J., & Colman, S. M. (2019). Late-Quaternary dynamics and palaeoclimatic implications of an alluvial fan-lake system on the southern Alxa Plateau, NW China. *Geomorphology*, *327*, 1–13. https://doi.org/10.1016/j.geomorph.2018.10.012

Yue, L., Juying, J., Bingzhe, T., Binting, C., & Hang, L. (2020). Response of runoff and soil erosion to erosive rainstorm events and vegetation restoration on abandoned slope farmland in the Loess Plateau region, China. *Journal of Hydrology*, *584*, 124694. https://doi.org/10.1016/j.jhydrol.2020.124694

Zielke, O., Klinger, Y., & Arrowsmith, J. R. (2015). Fault slip and earthquake recurrence along strike-slip faults—Contributions of high-resolution geomorphic data. *Tectonophysics*. https://doi.org/10.1016/j.tecto.2014.11.004

Zinelabedin, A., Riedesel, S., Reimann, T., Ritter, B., & Dunai, T. J. (2022). Testing the potential of using coarse-grain feldspars for post-IR IRSL dating of calcium sulphate-wedge growth in the Atacama Desert. *Quaternary Geochronology*, *71*, 101341. https://doi.org/10.1016/j.quageo.2022.101341